frontiers | Frontiers in Environmental Science

TYPE Original Research
PUBLISHED 30 August 2023
DOI 10.3389/fenvs.2023.1230983

OPEN ACCESS

EDITED BY
Joginder Singh,
Lovely Professional University, India

REVIEWED BY
Emad A. Elshehy,
Nuclear Materials Authority, Egypt
István Bányai,
University of Debrecen, Hungary

*CORRESPONDENCE
Prem C. Pandey,
pcpandey.apc@iitbhu.ac.in
Roger J. Narayan,
roger_narayan@unc.edu

RECEIVED 29 May 2023
ACCEPTED 14 August 2023
PUBLISHED 30 August 2023

CITATION
Pandey PC, Yadav HP, Tiwari AK, Sawant SN, Sinharoy P, Banerjee D and Narayan RJ (2023), Prussian blue nanoparticles–mediated sensing and removal of ^{137}Cs.
Front. Environ. Sci. 11:1230983.
doi: 10.3389/fenvs.2023.1230983

Prussian blue nanoparticles–mediated sensing and removal of ^{137}Cs

Prem C. Pandey[1]*, Hari Prakash Yadav[1], Atul Kumar Tiwari[1], Shilpa N. Sawant[2], Prithwish Sinharoy[3], Dayamoy Banerjee[3] and Roger J. Narayan[4]*

[1]Department of Chemistry, Indian Institute of Technology (BHU), Varanasi, India, [2]Chemistry Division, Bhabha Atomic Research Centre Trombay, Mumbai, India, [3]Process Development Division, Nuclear Recycle Group, Bhabha Atomic Research Centre Trombay, Mumbai, India, [4]Joint Department of Biomedical Engineering, University of North Carolina and North Carolina State University, Chapel Hill, NC, United States

Prussian blue nanoparticles (PBNPs) with controlled nano-geometry were synthesized from a single precursor (potassium hexacyanoferrate) in the presence of three different reagents, namely, polyethylenimine (PEI), tetrahydrofuran (THF)/H_2O_2, and 2-(3,4-epoxycyclohexyl)-ethyl-trimethoxysilane (EETMS)/cyclohexanone, which enabled the controlled nucleation and stabilization of PBNPs of variable plasmonic activities for selective sensing and removal of cesium radionuclides. The results of this study show the sensing and removal of cesium ions based on the nano-geometry, magnetic behavior, and fluorescence quenching ability of PBNPs as a function of the cesium ion concentration for the first time. A similar process was used to synthetically incorporate PBNPs in mesoporous silica with potential use for the selective adsorption of ^{137}Cs, followed by the detection of radioactivity. The distribution coefficient (Kd) for adsorption of the cesium nuclide ^{137}Cs was calculated to be 3.2 × 10^4 mL/g^{-1}, displaying both Langmuir and Freundlich adsorption isotherms. The plasmonic activity of PBNPs has enabled fluorometric sensing of cesium ions; regulating the spatial control between the functional PBNPs and fluorescence probe molecules is a promising approach for PBNP-enhanced fluorescence and fluorescence resonance energy transfer–based cesium ion sensing. Similarly, PBNPs display superparamagnetic behavior; these magnetic properties were observed to be linearly dependent on the cesium ion concentration.

KEYWORDS

Prussian blue nanoparticle, fluorescence sensing, selective adsorption, ^{137}Cs removal, fluorescence resonance energy transfer, superparamagnetic behavior

1 Introduction

The presence of radioactive cesium (^{137}Cs) in the environment has received increased attention from scientists and engineers after 940 TBq of radioactive cesium (^{137}Cs), which has a half-life of 30 years, entered the sea; this material poses a potential hazard since it emits strong gamma rays and beta particles that can affect living organisms. As a result, the removal of ^{137}Cs from contaminated water has been an ongoing focus of the research community (Yasunari et al., 2011; Yonekura et al., 2021); research efforts to remove ^{137}Cs from contaminated water have been documented by several researchers (Yasunari et al.,

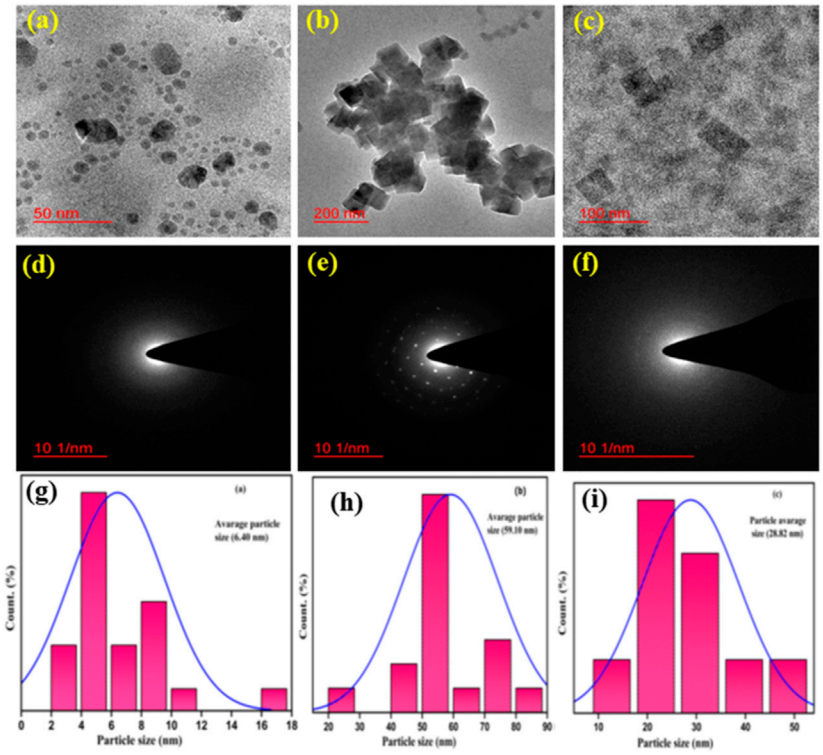

FIGURE 1
TEM characterization of synthesized PBNPs: **(A)** TEM image of PBNP-1, **(B)** TEM image of PBNP-2 and TEM image of PBNP-3, **(D)** SEAD pattern of PBNP-1, **(E)** SEAD pattern of PBNP-2, **(F)** SEAD pattern of PBNP-3, **(G)** size histogram of PBNP-1, **(H)** size histogram of PBNP-2, and **(I)** size histogram of PBNP-3.

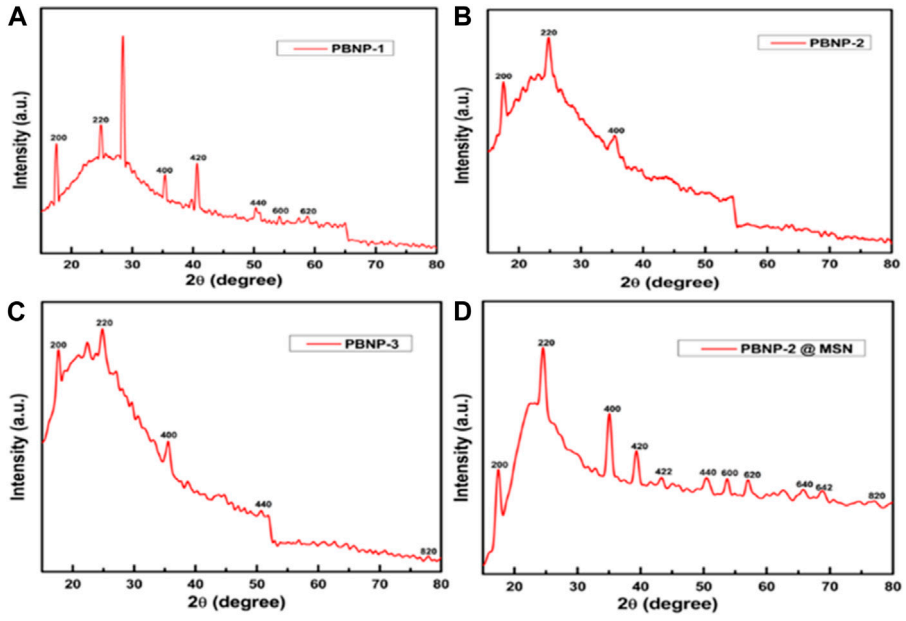

FIGURE 2
XRD data from **(A)** PBNP-1, **(B)** PBNP-2, **(C)** PBNP-3, and **(D)** PBNP-2@MSN.

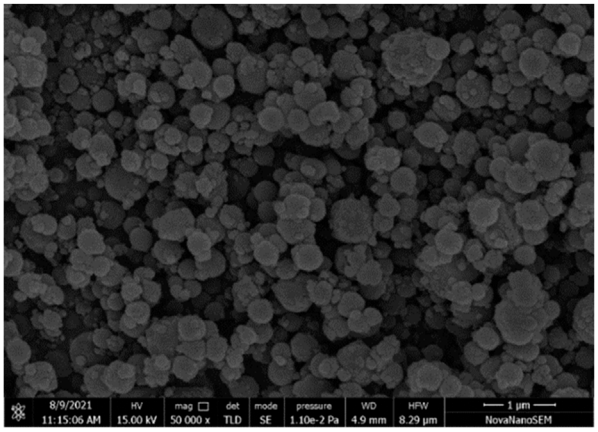

FIGURE 3
SEM image of PBNP-inserted mesoporous silica nanoparticles.

TABLE 1 Energy-dispersive X-ray spectroscopy of PBNP-2–inserted mesoporous silica nanoparticles (average size 200 nm).

Element	Weight%	Atomic%
Si K	98.94	99.47
Fe K	1.06	0.53
Totals	**100.00%**	

Bold value is total weight % of PBNP-2 incorporated mesoporous silica.

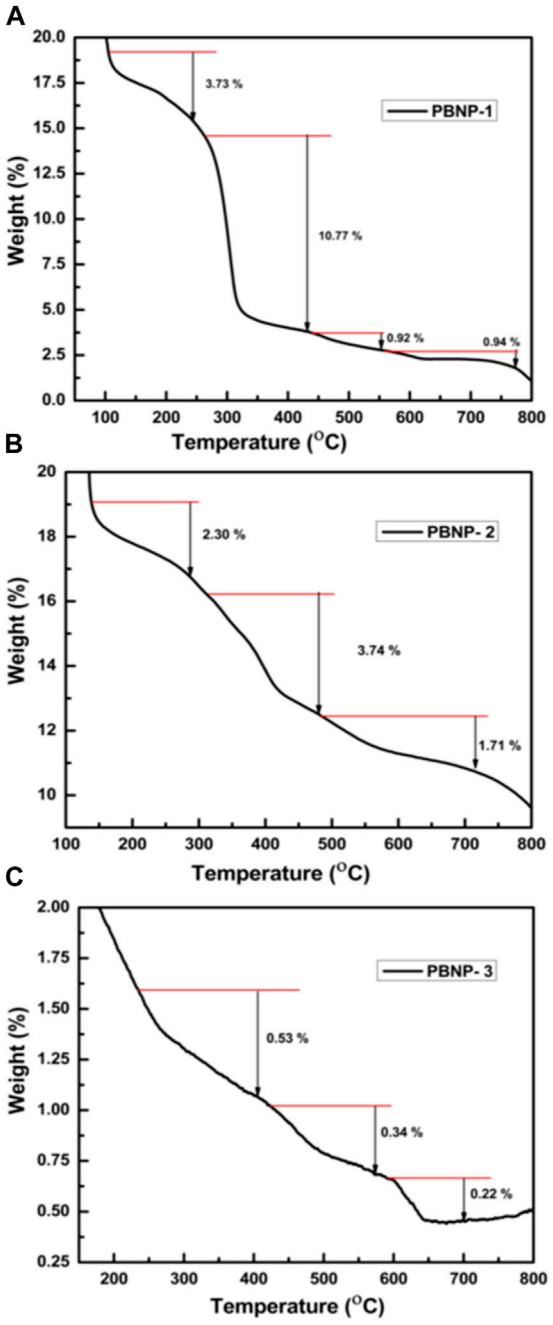

FIGURE 4
Thermogravimetric titration (TGA) of synthesized PBNPs: **(A)** PBNP-1, **(B)** PBNP-2, and **(C)** PBNP-3.

2011; Hu et al., 2012; Vipin et al., 2016; Kim et al., 2018; Faruque et al., 2019; Rauwel and Rauwel, 2019; Park et al., 2020; Estelrich and Busquets, 2021; Ohara et al., 2021; Yonekura et al., 2021). Apart from several reported adsorbents, there remains a requirement for biocompatible adsorbents that enable the removal of radioactive cesium from contaminated water. Prussian blue (PB), also known as ferric hexacyanoferrate, is an inorganic substance that shows a zeolite-like face-centered cubic lattice. This material has been shown to exchange potassium ions for cesium ions due to its high affinity to cesium in solution (Hu et al., 2012; Vipin et al., 2016; Kim et al., 2018; Faruque et al., 2019; Rauwel and Rauwel, 2019; Park et al., 2020; Estelrich and Busquets, 2021; Ohara et al., 2021); PB has been demonstrated as an antidote by the FDA. Previous studies have verified the active involvement of PB in cesium adsorption; the effectiveness of cesium removal is a function of parameters associated with PB and the additives used in making the adsorbent (Hu et al., 2012; Vipin et al., 2016; Kim et al., 2018; Faruque et al., 2019; Rauwel and Rauwel, 2019; Park et al., 2020; Estelrich and Busquets, 2021; Ohara et al., 2021). As such, these parameters have determined the activity of the material for the effective removal and sensing of cesium radionuclides. Since the PB nuclei are highly susceptible to undergo agglomeration and the subsequent crystalline morphology becomes insoluble in a variety of solvents, this phenomenon restricts the practical usability of the materials for cesium removal (Pandey and Pandey, 2012; Pandey and Pandey, 2013a; Pandey P. C. and Pandey A. K., 2013; Pandey and Pandey, 2013c; Pandey and Pandey, 2016; Pandey et al., 2018; Pandey et al., 2021a; Pandey et al. 2021b). Therefore, it is necessary to control the nano-geometry of PB nanoparticles (PBNPs) for the effective removal of ^{137}Cs. We have already demonstrated the controlled nucleation of PB made from single precursors in the presence of reagents; this approach allows for the controlled severance of potassium ferricyanide into ferrous ions that subsequently enable the formation of PBNPs, followed by the stabilization of the material (Pandey and Pandey, 2012; Pandey and Pandey, 2013a; Pandey P. C. and Pandey A. K.,

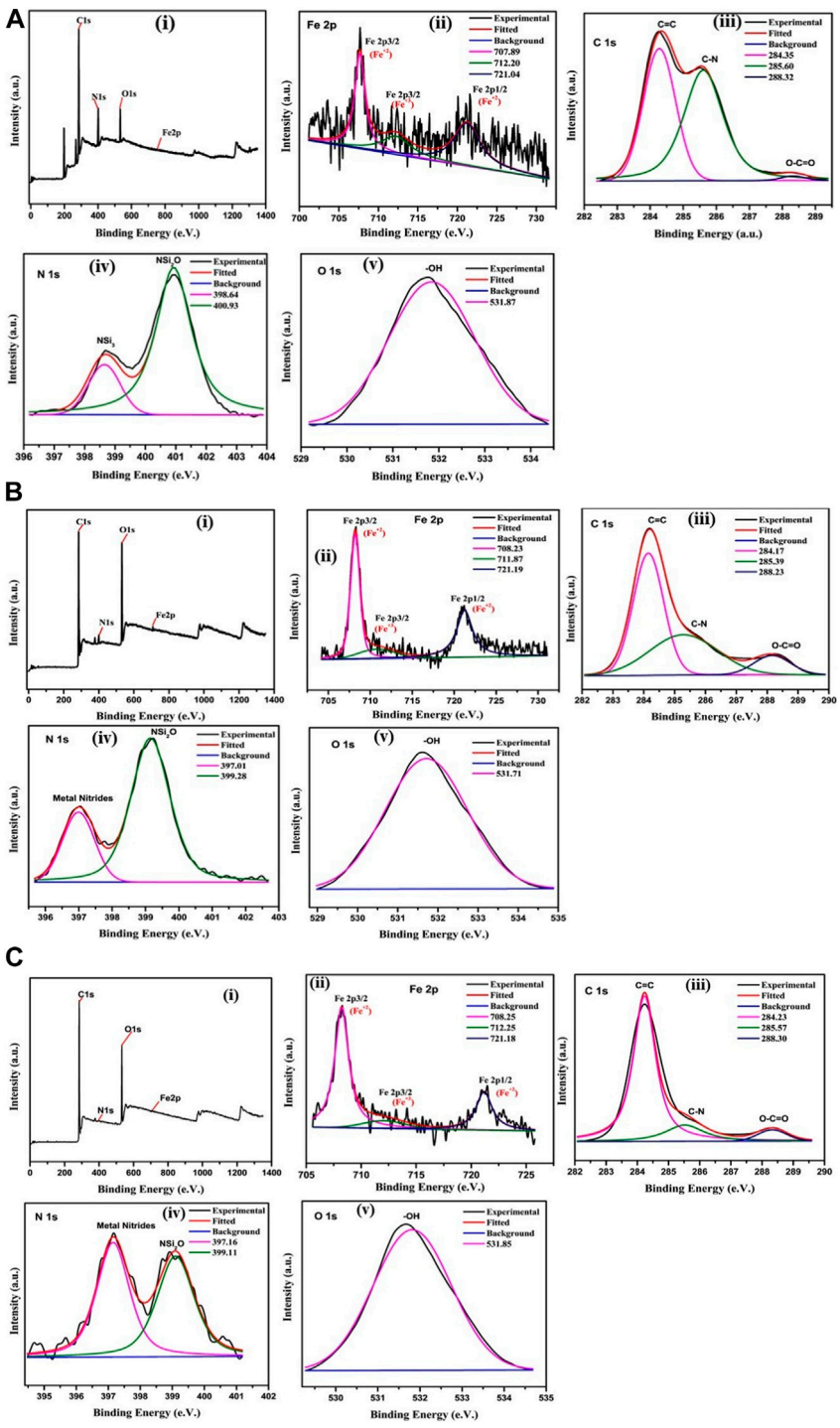

FIGURE 5
(A) XPS characterization of PBNP-1: **(i)** elemental scanning, **(ii)** Fe2p, **(iii)** C1s, **(iv)** N1s, and **(v)** O1s. **(B)** XPS characterization of PBNP-2: **(i)** elemental scanning, **(ii)** Fe2p, **(iii)** C1s, **(iv)** N1s, and **(v)** O1s. **(C)** XPS characterization of PBNP-3: **(i)** elemental scanning, **(ii)** Fe2p, **(iii)** C1s, **(iv)** N1s, and **(v)** O1s.

2013; Pandey and Pandey, 2013c; Pandey and Pandey, 2016; Pandey and Pandey, 2016; Pandey et al., 2018; Pandey et al., 2020; Pandey et al., 2021a; Pandey et al. 2021b). However, the role of nano-geometry on the adsorption characteristics of ^{137}Cs remains poorly understood. It has been shown that variations in the intensity of fluorescence of common fluorophores (e.g., fluorescein) can be attributed to distance effects and the surface plasmonic activity of the nanoparticles (Pandey et al., 2020). PBNPs display plasmonic activity and have been previously utilized as fluorescent quenchers (Pandey and Pandey, 2012; Pandey and Pandey, 2013a; Pandey and Pandey, 2016; Pandey et al., 2018; Pandey et al., 2021a; Pandey et al. 2021b). The reagents that are used to control the nucleation and

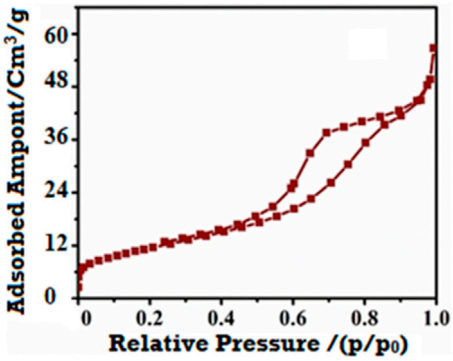

FIGURE 6
N_2 adsorption–desorption isotherms of PBNP-inserted mesoporous silica particles.

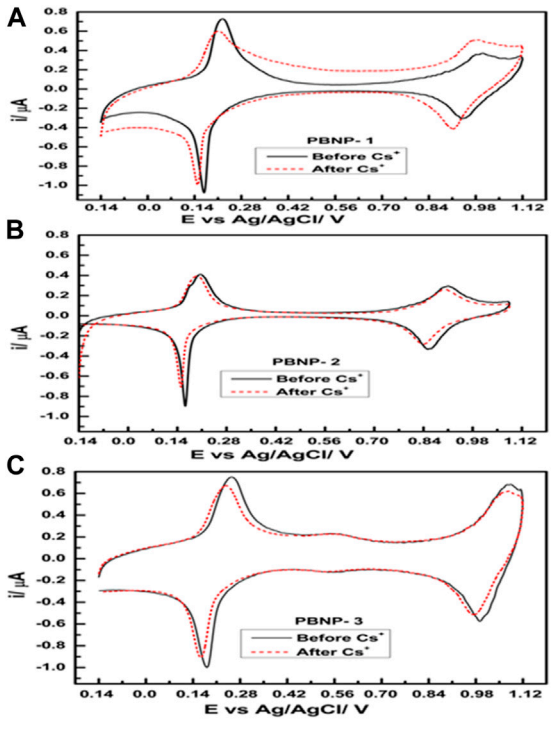

FIGURE 7
Cyclic voltammogram of **(A)** PBNP-1, **(B)** PBNP-2, and **(C)** PBNP-3 at a scan rate of 0.01 Vs^{-1} in 0.1 M KNO_3.

stabilization of PBNP-1, PBNP-2, and PBNP-3 may impart variable distance effects between a fluorescent probe molecule and nanoparticles and, as such, may be used for PBNP-mediated metal-enhanced fluorescence and fluorescence resonance energy transfer–based sensing of cesium radionuclides. A recent study justifies the formation of paramagnetic PB analogs CsM(II)[M(III)$(CN)_6$] (Kohler and Storcheva, 2015); in this study, MII and MIII are ions (transition metals) that are paramagnetic. Such events frequently entail fascinating magnetic properties such as ferri-3,4 and ferrimagnetism (Fornasieri et al., 2018). For PB containing alkali ions, the electron spins undergo spontaneous alignment up to slightly more than 100°C (Holmes and Girolami, 1999). Hence, these materials are referred to as room-temperature PB magnets and may display cesium ion concentration–dependent magnetic activity at room temperature.

Accordingly, the current study evaluates the synthesis of PBNPs with three different nano-geometries, namely, PBNP-1, PBNP-2, and PBNP-3, to understand the dependence of the nano-geometry of PB on cesium adsorption and sensing using several methodologies such as thermogravimetric analysis (TGA), fluorescence spectroscopy, cyclic voltammetry, X-ray fluorescence (XRF), and adsorption kinetics. Furthermore, exciting findings on the sensing and removal of cesium ions based on paramagnetic activity in both heterogeneous and homogenous formulations are reported in this study.

2 Experimental section

2.1 Materials and methods

Tetrahydrofuran, hydrogen peroxide, and cesium chloride were obtained from Sisco Research Laboratories Pvt. Ltd. (Mumbai, Maharashtra, India). Potassium ferricyanide was purchased from Sigma India (Bengaluru, Karnataka, India). The remaining chemicals (analytical grade) were obtained from commercial suppliers such as Sigma-Aldrich India (Bengaluru, Karnataka, India). Milli-Q water was utilized throughout the experiments.

2.2 Synthesis of nano-geometry controlled Prussian blue nanoparticles from single precursor

2.2.1 Polyethyleneimine (PEI)-mediated synthesis of PBNP-1

Up to 200 μL of $K_3[Fe(CN)_6]$ (0.05 M) aqueous solution and 65 μL of PEI (0.15 mg/mL) were blended under stirring over a vortex cyclomixer, followed by the addition of 10 μL HCl (6.5 M). The obtained mixture was incubated for 5 h at 60°C in an oven. The resultant yellow solution turned deep blue; this color change indicated the formation of PBNP-1.

2.2.2 THF-H_2O_2–mediated synthesis of PBNP-2

Two hundred microliters of aqueous solution of $K_3[Fe(CN)_6]$ (0.05 M) and 65 μL of (12 M) THF were mixed, followed by the addition of 130 μL of H_2O_2 (0.7 M; 30% w/v). The mixture was incubated for 2 h at 60°C in a hot air oven. The development of deep blue solution indicated the formation of PBNP-2.

2.2.3 2-(3,4-Epoxycyclohexyl)-ethyltrimethoxysilane and cyclohexanone-mediated synthesis of PBNP-3

Hundred microliters of aqueous solution of $K_3[Fe(CN)_6]$ (0.02 M) and 20 μL of 2-(3,4-Epoxycyclohexyl)-ethyltrimethoxysilane (EETMS) (0.2 M) were mixed, followed by drop-wise addition of 12 μL cyclohexanone (9.62 M). The mixture was incubated for 3 h at 60°C in an oven. The yellow solution turned deep blue, which indicated the formation of PBNP-3.

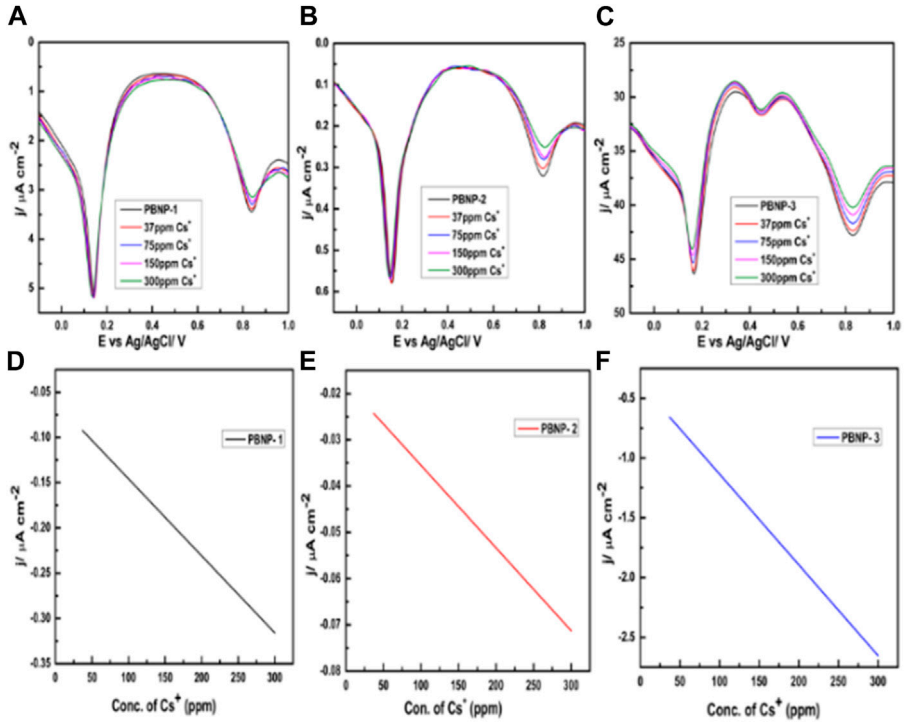

FIGURE 8
Study of electrochemical responses in the presence of Cs^+ (0–300 ppm) of **(A)** PBNP-1, **(B)** PBNP-2, and **(C)** PBNP-3; concentration-dependent calibration curves of Cs^+ for **(D)** PBNP-1, **(E)** PBNP-2, and **(F)** PBNP-3.

2.3 Synthetic incorporation of Prussian blue nanoparticles within mesoporous silica nanoparticles

A total of 120 mg of Mesoporous silica Nanoparticles (MSN) (200 nm) was suspended in 300 µL of an aqueous solution of K_3 [Fe $(CN)_6$] (0.65 M) and mixed over a cyclomixer for 3 h, followed by the collection of potassium hexacyanoferrate-inserted MSN by centrifugation. Potassium hexacyanoferrate-incorporated MSN were suspended in a reaction mixture containing 170 µL of THF (12 M) and 340 µL of H_2O_2 (0.7 M) under stirring over a cyclomixer and allowed to stand for 1.5 h, followed by incubation in an oven at 65°C for 6–7 h. The yellow mesoporous silica nanoparticles (MSNPs) turned deep blue, indicating the pore-inserted PBNPs. Furthermore, PBNP-inserted MSNPs were harvested by repeated centrifugation and washing with double distilled water.

2.4 Characterization of Prussian blue nanoparticles

The single precursor synthesis of PBNPs using potassium hexacyanoferrate in a homogeneous medium has been described previously (Pandey and Pandey, 2012; Pandey and Pandey, 2013a; Pandey P. C. and Pandey A. K., 2013; Pandey and Pandey, 2013c; Pandey and Pandey, 2016; Pandey et al., 2018; Pandey et al., 2020; Pandey et al., 2021a; Pandey et al. 2021b). Accordingly, the synthesized PBNPs were characterized using UV-Vis spectrometry (Hitachi U 2900, Tokyo Japan), TEM Tecnai G2 20 S TWIN (FEI, Hillsboro, Oregon, United States), X-ray diffraction (Rigaku MiniFlex 600 desktop XRD system, Japan), TGA (TGA 50, Simadzu Asia Pacific Pte Ltd, Singapore), and XPS (XPS K-alpha, ThermoFisher Scientific, United States). For TEM characterization, the PBNPs were diluted in Milli-Q water, followed by drop casting on a carbon-coated copper grid having a mesh size of 300, and visualized. A thin film of homogenous PBNPs casted on glass slide and powder of PBNP-2 incorporated mesoporous silica were processed for recording of X-Ray diffractogram. Additional characterization of PBNP-incorporated mesoporous silica was performed using a Nova NanoSEM 450 HR-SEM (FEI, Hillsboro, Oregon, United States) and X-ray fluorescence (XRF). Finally, a quantitative analysis of the specific surface area and porosity distribution of the PBNP-incorporated mesoporous silica was performed by using the Brunauer–Emmett–Teller (BET) analysis (BELLSORP MAX II and BELCAT-II, MicrotracBEL Corp., Osaka, Japan).

2.5 Electrochemistry of PBNP-1, PBNP-2, and PBNP-3–modified electrodes

The PBNP-1, PBNP-2, and PBNP-3–modified graphite paste were made by mixing PBNP-1/PBNP-2/PBNP-3, graphite powder, and Nujol oil. The process of paste fabrication involved mixing 5 µL of PBNP-1/PBNP-2/PBNP-3 with 9 mg spectroscopic grade graphite powder under sonication for 30 min, followed by drying overnight at 60°C in a vacuum oven. Furthermore, active PBNP-modified graphite paste was made by mixing graphite powder [68%

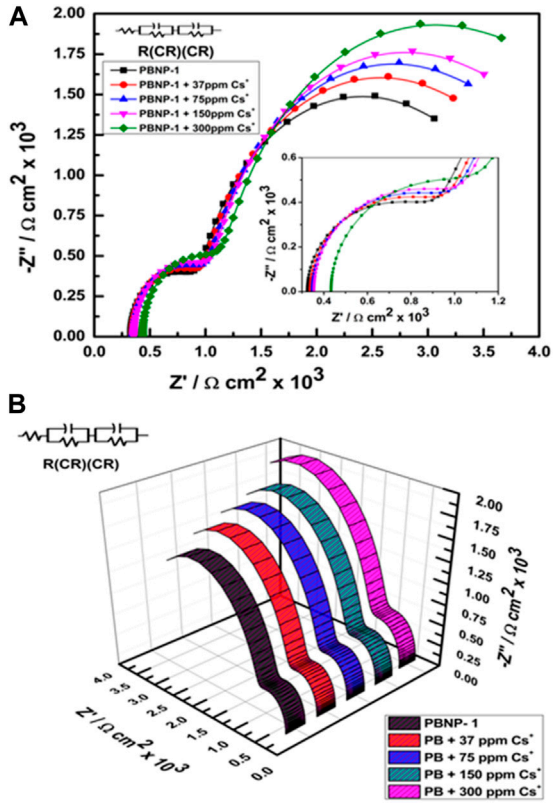

FIGURE 9
Nyquist plot of the PBNP-1–modified electrode **(A)** in the presence of varying concentrations of Cs^+ (0–300 ppm) and **(B)** 3D representation of the same.

TABLE 2 Dependence of R_{et} value of PBNPs on cesium ion concentration.

Cs^+ concentration/PB	PBNP-1 R_{et}	PBNP-2 R_{et}	PBNP-3
Blank (without Cs^+)	1.18×10^3	7×10^3	1.15×10^3
37 ppm	1.25×10^3	8×10^3	1.25×10^3
75 ppm	1.40×10^3	9×10^3	1.27×10^3
150 ppm	1.52×10^3	10×10^3	1.30×10^3
300 ppm	1.75×10^3	12×10^3	1.45×10^3

(w/w)], PBNP-adsorbed graphite [2.5% (w/w)], and Nujol oil [30% (w/w)]. The electrode body had a well with a recessed depth of 2 mm, which was packed with an active paste.

2.6 Electrochemical impedance spectroscopy

The stepwise construction of the PB-modified electrode was characterized using electrochemical impedance spectroscopy (EIS) in the absence and presence of cesium ions; this approach provided an efficient mechanism for investigating the interference properties of surface-limited electrodes. The impedance measurement was recorded on a CHI660B electrochemical workstation (CH Instruments, Inc., Austin, TX, United States); recordings were obtained between 1 Hz and 10 kHz at a suitable polarization potential. A semicircle section of the Nyquist plot representing charge transfer resistance and a linear section representing a diffusion-limited process are present in recordings obtained in the absence and presence of cesium ions. The almost straight line that the bare PBNP-modified electrode displayed in the electrochemical impedance spectroscopy (EIS) data can identify a diffusion-limiting stage of an electrochemical process. In this approach, the semicircle diameter corresponds to the electron transfer resistance (Ret). The usage of PBNP-mediated electrochemical sensing of cesium ions was justified by the semicircle diameter of the PBNP-modified electrode in the presence of cesium ions. The Nyquist diagram was plotted on the R(CR)(CR) circuit.

2.7 Fluorescence sensing of cesium ion–based PBNP-mediated fluorescence quenching of fluorescein

Cesium ion sensing was studied by fluorescence spectroscopy since PBNPs act as quenchers. Our previous study has demonstrated that functional PBNPs synthesized from 3-APTMS and cyclohexanone quench the *in situ* emission of fluorescence radiation within the visible range, demonstrating the quenching capability of PB (Pandey et al., 2020; Pandey et al., 2021a). However, the stability in the nano-geometry of PB is an important requirement for fluorescent quenching, as PB tends to agglomerate with time, converting the material to a photochemically inactive state (Pandey et al., 2020; Pandey et al., 2021b). Accordingly, the PBNPs, as reported herein as PBNP-1, PBNP-2, and PBNP-3, can be used as a fluorescence quencher of standard fluorophore: fluorescein. It is significant to note that PB refers to the formation of PBNPs from the use of a single precursor that is potassium ferricyanide, thus a double precursor is avoided, which allows an uncontrolled ratio of ferrous/ferric ions and hexacyanoferrate ions to yield a definite proportion of Fe II–C–N–Fe III within the polymeric network to precisely allow the interaction of cesium ions during the sensing process. A Hitachi F-7000 fluorescence spectrophotometer (Tokyo, Japan) was applied to measure the fluorescence in the samples. Since PBNPs behave as light quenchers, it is expected that the emission spectra of known luminescent/fluorescent materials may be significantly quenched in the presence of PBNPs. Fluorescein is chosen for such measurements since it is a well-known fluorescent material. Aqueous solutions of fluorescein of known concentration (10^{-7} M) were used under variable reaction conditions. Fluorescence sensing of cesium ions was recorded by monitoring the fluorescence spectra of (i) fluorescein only, (ii) fluorescein and metal PBNPs, (iii) fluorescein, PBNPs, and a variable concentration of cesium ions. The results showed that PBNP-1 made from the use of the cationic polymer polyethyleneimine yielded a cesium ion concentration–dependent fluorescence response when compared with that associated with PBNP-2 and PBNP-3, which is mainly attributed to fluorescence energy transfer in the presence of cesium

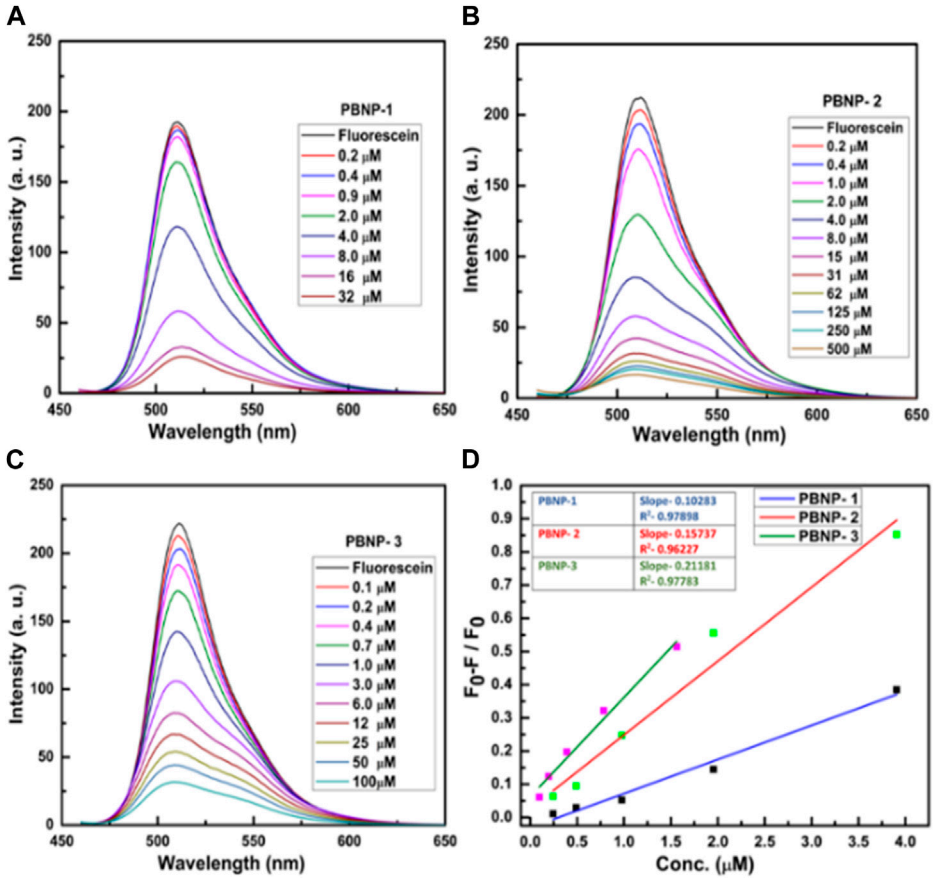

FIGURE 10
Dependence of fluorescence emission intensity on PBNP concentration between 0.1 and 500 mM for **(A)** PBNP-1, **(B)** PBNP-2, and **(C)** PBNP-3; **(D)** Stern–Volmer (S-V) plot shows the kinetic parameter of PBNPs.

ions with a cationic polymer as a spacer around PBNPs. The other two PBNPs did not show significant cesium ion concentration–dependent fluorescence quenching.

2.8 Prussian blue–incorporated mesoporous support for removal of cesium ions from contaminated water based on inductively coupled plasma resonance spectroscopy

The PBNPs inserted into a mesoporous support (50 mg) were incubated overnight with different concentrations of cesium ions between 1 ppm and 50 ppm. The adsorbed cesium ions over PBNP-incorporated mesoporous support were separated by centrifugation; the presence of cesium ions in the supernatant was monitored by using ICP spectroscopy. The Kd value was calculated to be 3.5×10^4 even at 3% PB content within the heterogeneous matrix. The PBNP-incorporated mesoporous support acted as a biocompatible adsorbent for cesium ion removal from contaminated water.

2.9 Measurement of ^{137}Cs radioactivity and determination of adsorption distribution coefficient (Kd)

The cesium uptake performance of the material was evaluated in a batch that was made by equilibrating 0.1 g of the sorbent and 10 mL of feed solution for 2 h at room temperature, followed by overnight standing. The batch distribution coefficient for Cs was measured using a test solution containing 5 g/L $NaNO_3$ spiked with ^{137}Cs radiotracer. To understand the ion exchange isotherm for Cs, test solutions of varying Cs concentrations ranging from 1 to 1,000 ppm were prepared by adding a requisite amount of $CsNO_3$ solution in 5 wt% $NaNO_3$ solutions and spiking them with ^{137}Cs tracer. The kinetics of the adsorption was studied using a feed solution having 10 ppm Cs spiked with ^{137}Cs tracer. In each case, after equilibration, the solution was filtered using a 0.2-micron syringe filter. The filtrate was analyzed for ^{137}Cs by counting with a NaI/Tl scintillation detector that was coupled to a single-channel analyzer.

10.3389/fenvs.2023.1230983

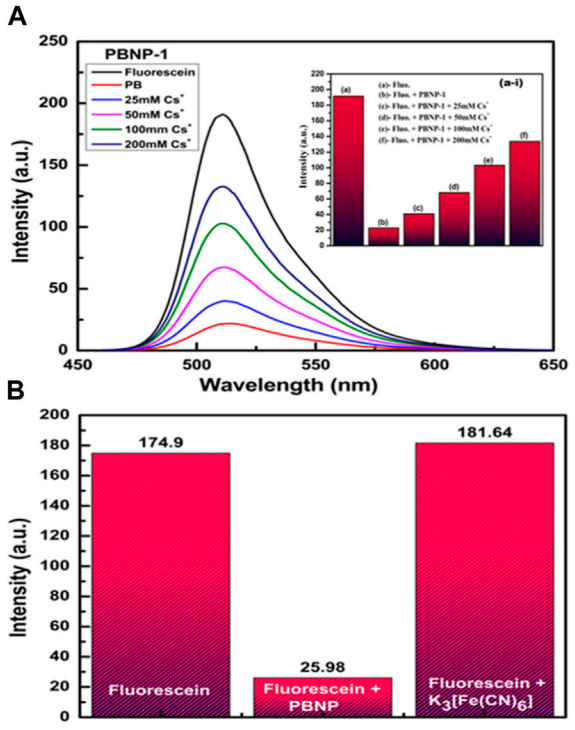

FIGURE 11
(A) Fluorescein in the absence and presence of different concentrations of Cs^+ (0–200 mM) and PBNP-1: (**a–i** inset) bar graph in the presence and absence of Cs^+ concentration with PBNP-1 and **(B)** fluorescein in the presence of PBNP and $K_3[Fe(CN)_6]$.

3 Results and discussion

3.1 Nano-geometry–controlled synthesis of Prussian blue nanoparticles (PBNP-1, PBNP-2, and PBNP-3)

The major objective of the current study was the nano-geometry–controlled synthesis of PBNPs with three different sizes depending on the reducing agent and to understand their impact on the sensing and removal of cesium ions. Since the traditional synthesis of PBNPs includes the agglomeration of nuclei into large particles, which is associated with poor processability, a good control over the synthetic strategy for PBNP formation is the first stage of the investigation (Pandey and Pandey, 2012; Pandey and Pandey, 2013a; Pandey P. C. and Pandey A. K., 2013; Pandey and Pandey, 2013c). Accordingly, the role of three different reagents, (i) PEI, (ii) THF and H_2O_2, and (iii) 2-(3,4-epoxycyclohexyl) ethyltrimethoxysilane and cyclohexanone, was evaluated. These reagents allowed for the controlled dissociation of potassium ferricyanide into a Fe^{++} derivative that subsequently interacted with potassium hexacyanoferrate, enabling the controlled nucleation of PB in two steps, followed by functionality as an efficient stabilizer to protect PB nano-geometry. The use of these reagents in PBNPs has already been demonstrated (Pandey and Pandey, 2012; Pandey and Pandey, 2013a; Pandey P. C. and Pandey A. K., 2013; Pandey and Pandey, 2013c). However, the use of these materials for the sensing and removal of cesium radionuclides has not been studied to this point. Accordingly, an investigation of the synthesis of PBNP-1, PBNP-2, and PBNP-3 as a homogeneous formulation for the sensing of cesium ions has been

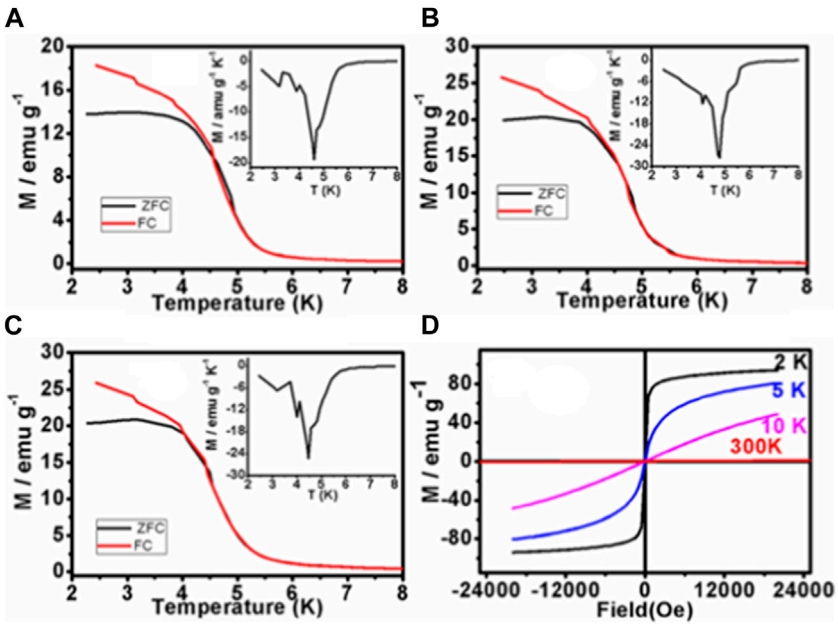

FIGURE 12
Normalized Zero-field cooled (ZFC) and field-cooled (FC) magnetization of PBNP-1 at the different applied fields (H): **(A)** 25 Oe, **(B)** 50 Oe, and **(C)** 100 Oe; **(D)** magnetization hysteresis loops at 2 K, 5 K, and 10 K, respectively.

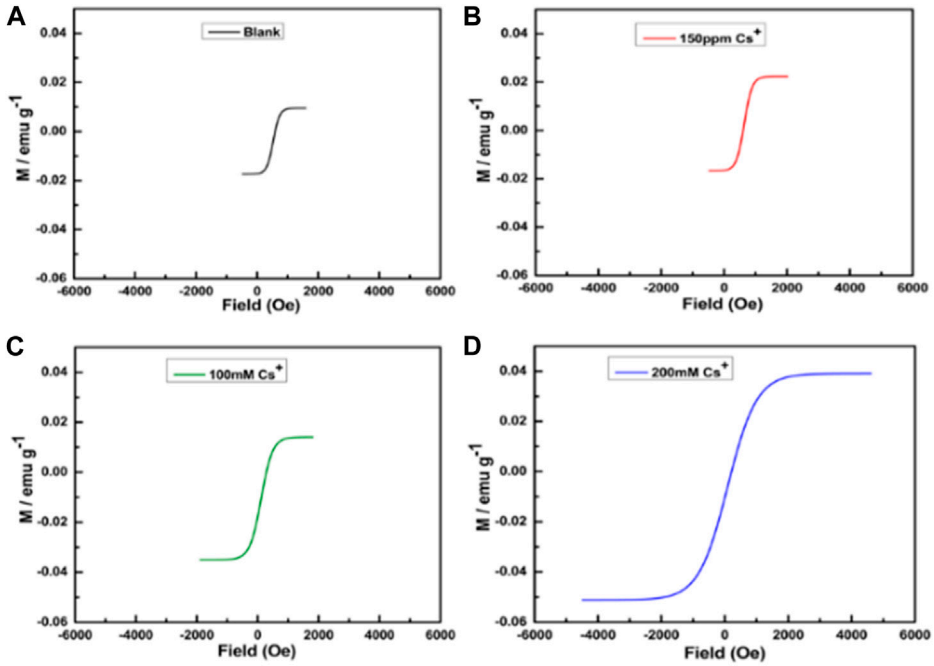

FIGURE 13
Magnetization hysteresis loops at 2 K of PBNP-1 at different concentrations of Cs^+: **(A)** without Cs^+, **(B)** 150 ppm, **(C)** 100 mM, and **(D)** 200 mM.

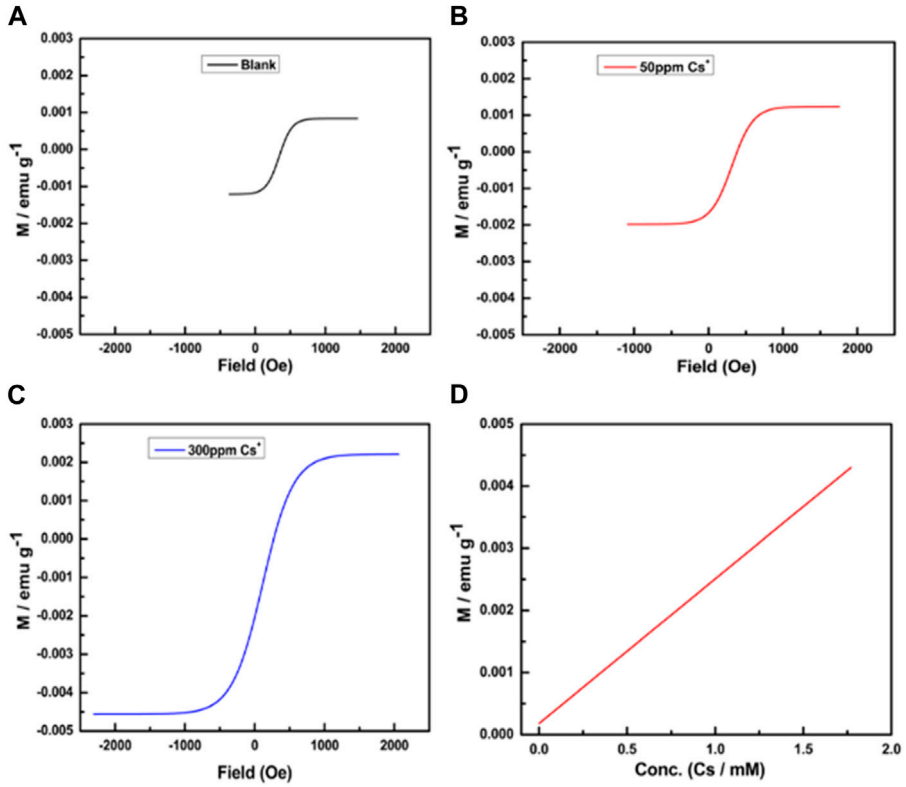

FIGURE 14
Magnetization hysteresis loops at 2 K of PBNP-2@MSN at different concentrations of Cs^+: **(A)** without Cs^+, **(B)** 50 ppm, **(C)** 300 ppm, and **(D)** calibration curve.

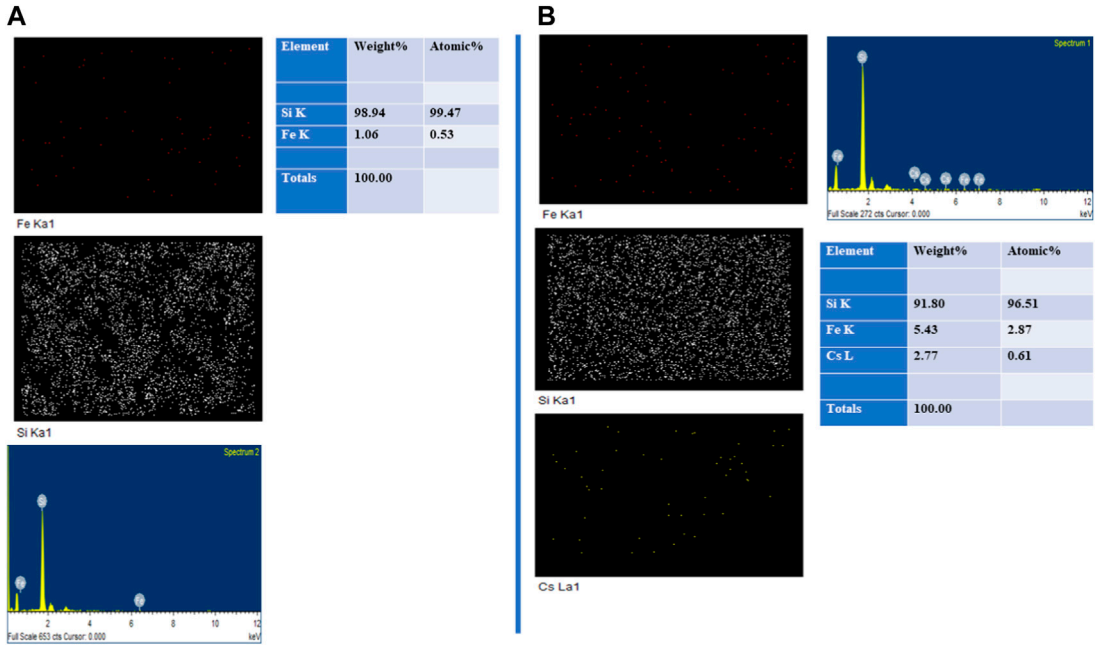

FIGURE 15
(A) Mapping analysis of PBNP-incorporated mesoporous silica in the absence of Cs^+; **(B)** mapping analysis of PBNP-incorporated mesoporous silica in the presence of Cs^+.

TABLE 3 ^{137}**Cs uptake performance of PBNP-encapsulated mesoporous silica (10% PBNPs w/w within MSNPs).**

Sample	Weight of the sample (g)	Volume of feed (mL)	V/M	Initial pH	Equi^m pH	Kd
10% PBNPs w/w within MSNPs	0.100	10	100.00	7.25	4.99	31,000 ± 1,500

demonstrated in this study. Further efficient removal of cesium radionuclides from contaminated samples essentially requires heterogeneous formations of PBNPs; by maintaining the nano-geometry of the PBNP-2 in the heterogeneous phase has been described. TEM characterization confirmed the size and shape of the as-made PBNPs, as shown in Figure 1. PBNP-1 was ~ 6.40 nm in size and spherical in shape (Figures 1A, D, G). PBNP-2 exhibited a rectangular shape and was ~ 60 nm in size (Figures 1B, E, H). PBNP-3 also exhibited a rectangular shape and size of ~ 28.8 nm (Figures 1C, F, I). Accordingly, the XRD results of the synthesized PB plane in both homogeneous and heterogeneous matrices were studied. Figures 2A–C show the XRD patterns for PBNP-1, PBNP-2, and PBNP-3, respectively. Figure 2D shows the XRD result for the PBNP-incorporated mesoporous silica support. According to Figures 2A–C, the strong and distinct peak was shown at 2θ values of 17.42, 24.96, 35.43, 39.54, 43.54, 50.72, and 54.03. The (200), (220), (400), (420), (422), (440), and (600) planes were allocated to these values, indicating an FCC lattice structure (JCPDS no. 73-0687). Since the XRD of the PBNP thin film on a glass surface was obtained, the diffractogram (as shown in Figures 2A–C) also indicates the presence of silica, as evidenced by a plateau at 2θ values between 20 and 25^0.

These reagents, particularly THF and H_2O_2, also enable the synthetic incorporation of PBNPs within mesoporous silica since they possess sufficient stability for efficient cesium ion removal. The XRD spectrum, as shown in Figure 2D, again confirms the presence of a sharp peak that was indexed with 2θ values of 17.42, 24.96, 35.43, 39.54, 43.54, 50.72, and 54.03^0, which are attributed to PB. The HR-SEM images of PBNP-2–incorporated mesoporous silica are shown in Figure 3; the presence of PBNP-2 in mesoporous silica was confirmed by using X-ray fluorescence (XRF), as shown in Table 1.

The thermogravimetric analysis (TGA) profiles for Prussian blue PBNP-1, PBNP-2, and PBNP-3 are shown in Figure 4. The thermal stability of the synthesized PBNPs was investigated using TGA. Figures 4A–C show the TGA results and depict four regions for PBNP-1 and three regions for PBNP-2 and PBNP-3 in which the PB lost weight. For PBNP-1, the first weight loss started at approximately 100°C and ended at 245°C; for PBNP-2, the weight loss occurred at 140°C and ended at 288°C. For PBNP-3, the weight loss started at 235°C and ended at 405°C; these findings can be related to intrinsically absorbed water molecules in the PB moiety being eliminated. The second weight loss for PBNP-1, PBNP-2, and PBNP-3 occurred at 260°C–430°C, 312°C–477°C, and 425°C to 572°C, respectively. The third weight loss for PBNP-1, PBNP-2, and PBNP-3 occurred at 441°C–554°C, 482°C–713°C, and 592°C–700°C, respectively. The fourth weight loss for PBNP-1, which occurred between 562°C and 774°C, was moderated and

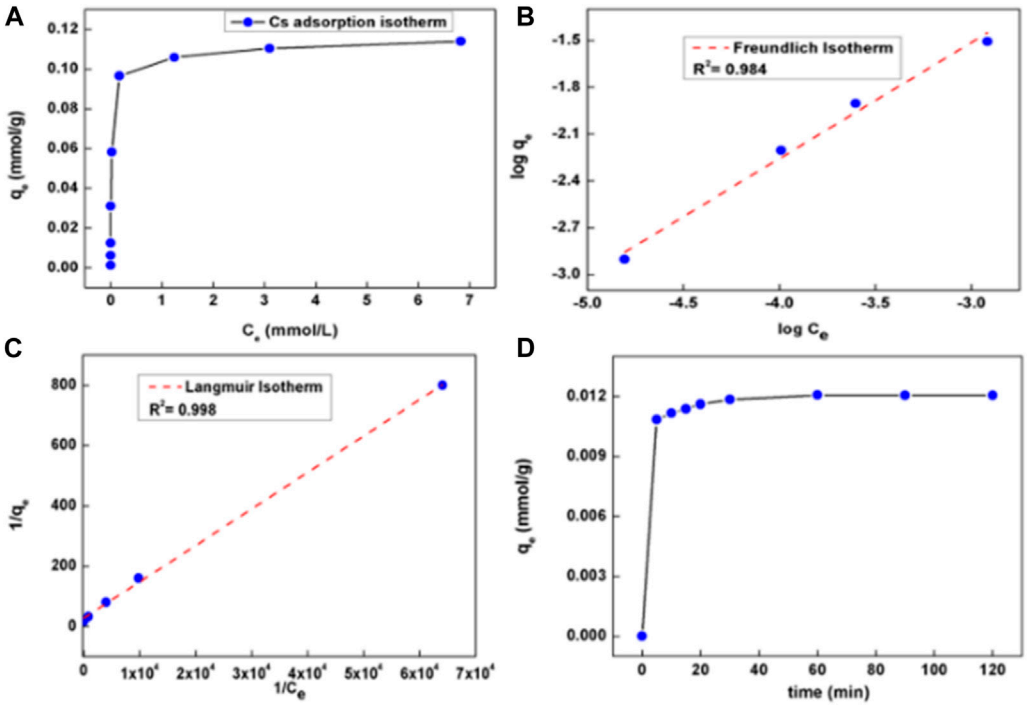

FIGURE 16
Cs^+ adsorption isotherm using **(A)** PBNP-incorporated silica, **(B)** fitting of Cs^+ adsorption using the Freundlich model, **(C)** fitting of Cs^+ adsorption using the Langmuir model, and **(D)** kinetics of cesium uptake using PBNP-incorporated silica.

TABLE 4 Comparison of previously reported LOD and maximum removal capacity of Cs^+ from water using PB.

Materials	Shape/size	LOD	Maximum removal capacity	References
Au@PB nanocomposite	1–6 μm	73.3 ppb	19.3 ppm	Namgung et al. (2018)
PB-embedded cellulose nanofiber	1–2 μm	1 mg/L^{-1}	54.2 mg g^{-1}	Park et al. (2023)
Mn-Fe PBA		0.013 mM		Zhou et al. (2021)
Prussian blue graphene hydrogel			4.67 mmol/g	Seema et al. (2023)
MBC-PB			52.3 mg/g	Park et al. (2023)
PAN-D-PB			186 mg/g	Gwon et al. (2020)
Prussian blue			500 ppb Cs^+	Ohara et al. (2021)
Magnetic Prussian blue/reduced graphene oxide			3.64 mmol/g	Seema (2020)
PB@Fe_3O_4 microparticles			16.13 mg/g	Wang et al. (2020)
PBNP-1/PBNP-incorporated mesoporous silica support	6 nm/200 nm	1.37 μM	0.1 mmol/g (13.29 mg/g)	This work

could be attributed to the presence of soluble and insoluble PBNPs. In PBNP-1, the mass losses at steps I, II, III, and IV were 3.73%, 10.77%, 0.92%, and 0.94%, respectively. In PBNP-2, the mass losses at steps I, II, and III were 2.30%, 3.74%, and 1.71%, respectively. In PBNP-3, the mass losses at steps I, II, and III were 0.53%, 0.34%, and 0.22%, respectively. In step I, mass reductions were attributed to water loss in the PB structure; mass losses in steps II, III, and IV were correlated with the release of cyanide groups from the PB structure.

3.2 XPS of PBNP-1, PBNP-2, and PBNP-3

XPS analysis was conducted on PBNP-1, PBNP-2, and PBNP-3 under ambient conditions. The analysis of the XPS data indicated the existence of both Fe (II) and Fe (III) species in the PBNP samples that were synthesized. The binding energies of PBNP-1, PBNP-2, and PBNP-3 were measured to be 721.04 eV and 707.89 eV, 721.29 eV and 708.25 eV, and 721.18 eV and 708.25 eV, respectively; these values correspond to the Fe 2p1/2 and Fe 2p3/

2 orbitals. The observed peaks serve as empirical support for the existence of the distinctive Fe^{2+} moiety within PB. Furthermore, the identification of peaks at binding energies (BEs) of 712.82 eV for PBNP-2, 711.87 eV for PBNP-2, and 712.25 eV for PBNP-3 provides evidence for the existence of Fe^{+3} entities. The X-ray photoelectron spectroscopy (XPS) analysis of all three PBNPs demonstrates that PBNP-1 exhibits a noticeably higher intensity in comparison to PBNP-2 and PBNP-3 [as seen in Figures 5A–C].

The surface area and pore diameter of the as-synthesized catalyst were examined via BET analysis. The N_2 adsorption–desorption isotherms of PBNP-2–incorporated mesoporous silica are shown in Figure 6. The PBNP-incorporated mesoporous silica exhibited a type-IV isotherm; a 40.3 m^2/g specific surface area and 7.14 nm pore width were determined according to the adsorption–desorption curve. These results justify controlling the nanoscale features of chemically synthesized PB and the formation of PBNP-incorporated mesoporous silica supports for subsequent removal applications.

3.3 Electrochemical sensing of cesium ions

3.3.1 Cyclic voltammetry

Initially, we examined the sensing of cesium ions through the electrochemical behavior of PB-modified electrodes via cyclic voltammetry. PB displays two redox peaks; the first one is recorded at 0.2 V, which is attributed to Prussian white oxidation to PB reduction, and *vice versa*. By contrast, the second redox couple that appears at 0.9 V corresponds to PB oxidation to Berlin green reduction, and *vice versa*. Accordingly, we first examined the dependence of this redox-active reaction as a function of cesium ion concentrations. A typical voltammogram of PBNP-1/PBNP-2/PBNP-3–modified electrode in the presence and absence of 1 mM cesium ions is provided in Figure 7. The results demonstrate inconclusive findings on the dependence of the first redox peak as a function of the cesium ion concentration; however, some insights related to the dependence of the second redox couple on the cesium ion concentration were noted. Accordingly, we further attempted to record differential pulse voltammetry to obtain insights related to cesium ion sensing. Electrochemical sensing of cesium ions with PBNP-1/PBNP-2/PBNP-3–modified electrodes was evaluated from differential pulse voltammetry recorded between −0.2 V and 1.0 V vs. Ag/AgCl, as shown in Figure 8. Notably, the second redox couple of PB was found to be dependent on cesium ions; the peak current decreased with an increase in cesium ion concentration. All the three PB-modified electrodes (PBNP-1/PBNP-2/PBNP-3) displayed similar behavior, with a sensitivity of approximately 8.5×10^{-4}, 1.8×10^{-4}, and 7.5×10^{-6}, respectively; these results indicate a better sensing functionality of the PBNP-1–modified electrode.

3.3.2 Electrochemical impedance spectroscopy

Figure 9 displays the electrochemical impedance spectroscopy results from the modified PBNP electrode in the presence and absence of several concentrations of cesium ions. The semicircle section of the impedance spectra depicted in Figure 9A corresponds to charge transfer resistance; the linear section of the spectra corresponds to a diffusion-limited process. The nearly straight line indicates the diffusion-limiting step of the electrochemical process that the EIS of the bare PBNP-modified electrode (Figure 8) displays. The diameter of the semicircle and the electron-transfer resistance (Ret) are related. In contrast to the PBNP-modified electrode in the presence of cesium ions (Figure 9), the semicircle diameter for the PBNP-modified electrode tends to increase. The charge transfer resistance increased with increase in cesium ion concentrations, as shown in Table 2; this result indicates that the predominantly diffusion-limiting step of the electrochemical process takes place between the PBNPs and Cs ions.

3.4 Fluorometric sensing of cesium ions

The optical properties of PB show broad optical adsorption over 550 nm–800 nm, corresponding to the blue region. It should be noted that fully oxidized PBNP thin films exhibit a lower absorption peak at 760 nm. However, in its fully reduced state, PW absorbs quite weakly in the visible region, resulting in a transparent state. The optical absorption coefficient value of a semiconductor may be represented by its direct/indirect optical band gap. The band gaps previously recorded by Qiu et al. (2020) for PB, PY, and PW have been described in the order of 1.75 eV, 2.02 eV, and 3.53 eV, respectively; these parameters indicate that the optoelectronic properties of PB-related compounds should be controlled for cesium ion sensing. We have previously reported that PBNPs act as fluorescence quenchers (Pandey et al., 2020; Pandey et al., 2021a). Accordingly, we investigated the fluorescence quenching ability of the well-known fluorophore fluorescein, which exhibits excitation and emission spectra at 494 and 521 nm, respectively. Figure 10 shows the fluorescence quenching ability of PBNP-1, PBNP-2, and PBNP-3 on fluorescein emission (Figures 10A–C). This finding clearly predicts excellent fluorescence quenching of PBNPs with a quenching constant as calculated from the Stern–Volmer (S-V) plot (Mitra and Pandey, 2022). The values of the quenching constant were found to be 10,283 M^{-1} s^{-1}, 15,737 M^{-1} s^{-1}, and 21,181 M^{-1} s^{-1} for PBNP-1, PBNP-2, and PBNP-3, respectively, as indicated in Figure 10D; these results confirm the excellent quenching functionality of the as-made PBNPs. PBNPs cause efficient quenching of fluorescein fluorescence; this phenomenon is likely due to the energy transfer process between fluorescein as the donor and PBNPs as the acceptor. In stable functional PBNPs made using PEI/organotrialkoxysilane/THF + H_2O_2 as the reagent, the reagent protects the nano-geometry of PBNPs for specific applications and behaves as a specific spacer to meet the requirement of energy transfer, as has been previously discussed (Pandey et al., 2020; Pandey et al., 2021b). Accordingly, we further investigated the variation of the fluorescence quenching functionality of the as-made PBNPs in the presence of cesium ions. Notably, PBNP-2 and PBNP-3 showed very poor variation in the fluorescence quenching of fluorescein as a function of cesium ions; on the other hand, PBNP-1 displayed cesium ion concentration–dependent quenching functionality, as shown in Figure 11. The quenching ability of PBNP-1 decreased with increasing cesium ion concentrations. The reason behind this variation might be associated with the charge available around the spacer that might alter the quenching ability of PBNPs in the presence of charged cesium ions. The neutral spacer may not

participate in altering the field quenching ability of PBNP; on the other hand, the charged spacer-like cationic polymer PEI may alter the quenching ability of PBNPs. Since PBNP-1 is derived from a cationic polymer, polyethyleneimine, an excellent result of the decrease in quenching ability of PBNP-1 has been recorded as a function of cesium ion concentration (Figure 11A). A linear relationship between cesium ion concentration and quenching extent in terms of percentage quenching of PBNPs was recorded, as shown in Figure 10D, justifying the innovative results from cesium ion sensing via fluorescence measurements. We further examined the difference in the quenching ability of PBNPs and $K_3[Fe\ (CN)_6]$, if any, to understand the impact of making PBNPs from the single precursor potassium ferricyanide (Figure 11B). Figure 11B shows the results of this study, which indicate that $K_3[Fe\ (CN)_6]$ is not a fluorescent quencher, and confirms the requirement of both MII and MIII Fe ions for fluorescence quenching functionality.

3.5 Sensing of cesium ions based on magnetic measurements

The name "Prussian blue" refers to polynuclear hexacyanometallates, which have a cubic crystal structure with a three-dimensional ....N-MIII-N-C-MII-C.... configuration and form a supramolecular network. If MII and MIII are paramagnetic transition metal ions, then they introduce magnetic properties such as ferri-3,4 and ferromagnetism (Kohler and Storcheva, 2015). Accordingly, PBNPs may display superparamagnetic characteristics as a function of temperature, as shown in Figure 12. The synthesized PBNPs displayed superparamagnetism with high saturation, zero coercivity, and remanence, as shown in Figure 12A; M(T) for zero field cooling (ZFC) is shown in Figure 12B; and the field cooling (FC) program is shown in Figure 12C at different field strengths (i.e., 25, 50, and 100 Oe) with blocking temperatures of 4.3 K, 4.4 K, and 4.2 K as appropriate for a superparamagnetic material. Magnetization hysteresis loops at 2 K, 5 K, and 10 K are shown in Figure 12D, again justifying the superparamagnetic characteristics.

Even at room temperature, the paramagnetic behavior is relatively low. Cesium ions residing in the cubic holes of the lattice may balance out the charge differences between MII and MIII, altering the paramagnetic properties. Accordingly, we investigated the change in the paramagnetic ability of PBNPs as a function of cesium ion concentration. Notably, the paramagnetic functionality of PBNPs in both homogeneous and heterogeneous phases (within the mesoporous matrix) is altered dramatically in the cesium ions; this result provides excellent information on the sensing and removal of cesium ions based on PBNP formulation in the homogeneous and heterogeneous phases. Figure 13 displays the variation in the magnetic property of PBNP powder as a function of cesium ion concentration, indicating the dependence of the paramagnetic character of PBNPs on cesium ion concentration. Furthermore, the PBNPs present in heterogeneous phases, especially within mesoporous silica nanoparticles, may serve as a potential adsorbent for cesium ion removal; accordingly, we investigated the ability of PBNP-incorporated mesoporous silica for cesium ion sensing based on magnetic measurements. Cesium ions of variable concentrations of 10–600 ppm were incubated with PBNP-incorporated mesoporous silica, followed by collection of the heterogeneous matrix, washing, and drying. The magnetic measurement of cesium-adsorbed PBNPs within mesoporous silica was examined, as shown in Figure 14. The results clearly indicate that the magnetic properties of PBNPs vary as a function of cesium ion concentration, which is associated with an increase in unpaired electrons in PBNPs. These findings provide insights into the effective adsorbent behavior of PBNP-incorporated mesoporous silica in radioactive cesium removal from contaminated water.

3.6 ^{137}Cesium ion removal

One of the major tasks of the current study was to evaluate the materials for use as an efficient biocompatible matrix for ^{137}Cs removal from contaminated water. Adsorption is a cost-effective approach to remove cesium ions from contaminated water. The transport of cesium from contaminated water to the surface of a solid matrix is implied by this separation process (i.e., PBNP-incorporated mesoporous silica as an adsorbent). A material for this application should possess a tailored surface chemistry and porosity to obtain effective cesium ion separation (as evident from Figure 3); this approach justifies the synthetic incorporation of PBNPs within mesoporous silica. The results recorded in Figure 2 on XRD and PBNP-incorporated mesoporous silica and the BET results shown in Figure 6 clearly confirm the formation of a PBNP-incorporated mesoporous silica matrix as a potential ^{137}Cs ion adsorbent. After the magnetic measurements were obtained, we examined the binding ability of PBNP-incorporated mesoporous silica–based materials using energy dispersive X-ray analysis. Figure 15 shows the findings from the adsorption of cesium ions at different concentrations that were present in contaminated water. The data were obtained in the absence of cesium ions (Figure 15) and in the presence of 300 ppm cesium ions. Figure 15 clearly confirms the efficient binding ability of PBNP-incorporated mesoporous silica for cesium ion removal. These findings are further confirmed by the measurement of cesium ions in the supernatant of these four samples by Inductive coupled plasma Emission spectroscopy (ICPE). The results have clearly confirmed the efficiency of PBNP-incorporated mesoporous silica, which was noted to be highly suitable for the removal of cesium ions.

We have further examined the functionality of PBNP-incorporated mesoporous silica for the removal of cesium ions based on the measurement of radioactivity of ^{137}Cs ions. The adsorption coefficient of PBNP-incorporated mesoporous silica based on the radioactivity measurement of ^{137}Cs was calculated to be 3.5×10^4 even at 3% PB content within the heterogeneous matrix, justifying the efficiency of the material for radioactive cesium removal, as shown in Table 3. Figure 16A shows the cesium adsorption isotherm of PBNP-incorporated mesoporous silica over an equilibrium Cs concentration range of 1–1,000 ppm. Almost all of the Cs was taken up by the material at lower cesium concentrations, followed by a sharp increase beyond 0.001 M Cs, indicating occupancy of all of the sites by Cs. Flattening of the curve beyond 0.001 M Cs signifies the attainment of equilibrium Cs uptake capacity. The maximum Cs sorption capacity (qe mmol/g) of the sorbent was calculated to be

0.1 meq/g, which is in good agreement with previously reported values, as compared in Table 4. The previously described adsorption isotherm was fitted using both the Freundlich and Langmuir adsorption isotherm models, shown in Figures 16B, C. The fitting parameters were obtained to provide a mechanistic understanding of the surface properties and affinity of the sorbent. The Freundlich and Langmuir isotherm model equations can be represented as follows:

$$\textbf{In the Freundlich model: } \ln q_e = \ln K_F + \frac{1}{n}\ln C_e \quad \text{.....} \quad (1)$$

where K_F denotes the sorption capacity when the metal ion equilibrium concentration is equal to 1, and 1/n denotes the degree of sorption dependency with the equilibrium concentration.

$$\textbf{In the Langmuir model: } \frac{1}{q_e} = \frac{1}{q_m} + \frac{1}{K_L C_e q_m} \quad \text{.....} \quad (2)$$

where q_m and K_L are the maximum monolayer capacity and sorption coefficient, respectively.

As per the fitting with the Freundlich model, the adsorption data show a linear relationship (R^2 = 0.98); the values of K_F and "*n*," as obtained from the log–log plot, were found to be 5.23 and 1.34, respectively. This "*n*" value indicates a monolayer adsorption of Cs taking place on the sorbent surface. Similarly, the fitting with the Langmuir model (R^2 = 0.99) culminated in q_e and K_L values of 0.037 mmol/g and 2,280, respectively.

A study on the kinetics of adsorption is important for optimizing uptake performance. Hence, the sorbent was in contact with 10-ppm Cs solution for different time intervals; the uptake capacity of the sorbent as a function of time is shown in Figure 16D. It can be inferred that equilibrium is attained within 20 min of maximum uptake capacity.

4 Conclusion

PBNPs of controlled nano-geometry were synthesized using a single precursor and different organic reducing agents and reported in homogeneous and heterogeneous mesoporous silica support for efficient sensing and removal of ^{137}Cs ion from water. Cesium ion sensing based on differential pulse voltammetry and impedance spectroscopy was demonstrated. The results were described based on the fluorescence quenching ability of PBNPs made from single precursors. The quenching ability of PBNPs was noted to be a function of the nano-geometry of the PBNPs. Furthermore, when cationic polymers are used to stabilize PBNPs, the quenching ability of PBNPs depends on the concentration of cesium ions, justifying the fluorescence sensing of the same. PBNPs in both homogeneous and heterogeneous phases display paramagnetic behavior, which was noted to be a function of the cesium ion concentration. The fast kinetics and high uptake capacity of the PBNP-incorporated mesoporous silica make this material a suitable matrix for removing ^{137}Cs from contaminated water; this study suggests subsequent efforts to prepare granular beads that can be used in the column mode.

Data availability statement

The raw data supporting the conclusion of this article will be made available by the authors, without undue reservation.

Author contributions

PP conceived and designed the experiments. HY, AT, and PS conducted the sample preparation and the experiments. PP, SS, and DB wrote the manuscripts and analyses. RN and PP oversaw the completion of this study and edited the manuscript. All authors contributed to the article and approved the submitted version.

Acknowledgments

The authors are grateful to the Central Instrument Facility, Indian Institute of Technology (BHU), for the characterization of nanoparticles.

Conflict of interest

The authors declare that the research was conducted in the absence of any commercial or financial relationships that could be construed as a potential conflict of interest.

Publisher's note

References

Estelrich, J., and Busquets, M. A. (2021). Prussian blue: a safe pigment with zeolitic-like activity. *Int. J. Mol. Sci.* 22, 780. doi:10.3390/ijms22020780

Faruque, H. A., Choi, E. S., Kim, J. H., Kim, S., and Kim, E. (2019). *In vivo* removal of radioactive cesium compound using Prussian blue-deposited iron oxide nanoparticles. *Nanomedicine* 14, 3143–3158. doi:10.2217/nnm-2019-0085

Fornasieri, G., Bordage, A., and Bleuzen, A. (2018). Magnetism and photomagnetism of prussian blue analogue nanoparticles embedded in porous metal oxide ordered nanostructures. *Eu. J. inor. che.* 2018, 259–271. doi:10.1002/ejic.201700819

Gwon, Y. J., Lee, J. J., Lee, K-W., Ogden, M. D., Harwood, L. M., and Lee, T. S. (2020). Prussian blue decoration on polyacrylonitrile nanofibers using polydopamine for effective Cs ion removal. *Industrial Eng. Chem. Res.* 59 (11), 4872–4880. doi:10.1021/acs.iecr.9b06639

Holmes, S. M., and Girolami, G. S. (1999). Sol-gel synthesis of KVII [CrIII(CN)$_6$] 2H$_2$O: a crystalline molecule-based magnet with a magnetic ordering temperature above 100 °C. *A C S* 121, 5593–5594. doi:10.1021/ja990946c

Hu, M., Furukawa, S., Ohtani, R., Sukegawa, H., Nemoto, Y., Reboul, J., et al. (2012). Synthesis of Prussian blue nanoparticles with a hollow interior by controlled chemical etching. *Angew. Chem. Int. Ed. Engl.* 51, 984–988. doi:10.1002/anie.201105190

Kohler, F. H., and Storcheva, O. (2015). Paramagnetic prussian blue analogues $CsM(II)[M(III)(CN)_6]$. The quest for spin on cesium ions by use of (133) Cs MAS NMR spectroscopy. *Inorg. Chem.* 54, 6801–6806. doi:10.1021/acs.inorgchem.5b00711

Kim, H., Kim, M., Lee, W., and Kim, S. (2018). Rapid removal of radioactive cesium by polyacrylonitrile nanofibers containing Prussian blue. *J. Haz. Mat.* 347, 106–113. doi:10.1016/j.jhazmat.2017.12.050

Mitra, M. D., and Pandey, P. C. (2022). Functional trialkoxysilane mediated controlled synthesis of fluorescent gold nanoparticles and fluoremetric sensing of dopamine. *Opt. Mater.* 132, 112810. doi:10.1016/j.optmat.2022.112810

Namgung, H., Gwon, Y. J., Kim, J., Jang, G., Pepper, S. E., Ogden, M. D., et al. (2018). Synthesis of Prussian blue-embedded porous polymer for detection and removal of Cs ions. *Polymer* 158, 320–326. doi:10.1016/j.polymer.2018.11.001

Ohara, E., Soejima, T., and Ito, S. (2021). Removal of low concentration Cs (I) from water using Prussian blue. *Inorganica. Chim. Acta.* 514, 120029. doi:10.1016/j.ica.2020.120029

Pandey, P. C., and Pandey, A. K. (2012). *Indian Pat.*, 295327.

Pandey, P. C., and Pandey, A. K. (2013c). Cyclohexanone and 3-aminopropyltrimethoxysilane mediated controlled synthesis of mixed nickel-iron hexacyanoferrate nanosol for selective sensing of glutathione and hydrogen peroxide. *Analyst* 138, 952–959. doi:10.1039/C2AN36228G

Pandey, P. C., and Pandey, A. K. (2013b). Novel synthesis of Prussian blue nanoparticles and nanocomposite sol: electro-analytical application in hydrogen peroxide sensing. *Electrochimica Acta* 87, 1–8. doi:10.1016/j.electacta.2012.08.069

Pandey, P. C., and Pandey, A. K. (2013a). Novel synthesis of super peroxidase mimetic polycrystalline mixed metal hexacyanoferrates nanoparticles dispersion. *Analyst* 138, 2295. doi:10.1039/C3AN00060E

Pandey, P. C., and Pandey, D. (2016). Tetrahydrofuran and hydrogen peroxide mediated conversion of potassium hexacyanoferrate into Prussian blue nanoparticles: application to hydrogen peroxide sensing. *Electrochimica Acta* 190, 758–765. doi:10.1016/j.electacta.2015.12.188

Pandey, P. C., Shukla, S., and Narayan, R. J. (2021a). Organotrialkoxysilane-Functionalized prussian blue nanoparticles-mediated fluorescence sensing of arsenic (III). *Nanomaterials* 11, 1145. doi:10.3390/nano11051145

Pandey, P. C., Shukla, S., Pandey, G., and Narayan, R. J. (2020). Organotrialkoxysilane-mediated controlled synthesis of noble metal nanoparticles and their impact on selective fluorescence enhancement and quenching. *J. Vac. Sci. Tech. B* 38, 052801. doi:10.1116/6.0000334

Pandey, P. C., Singh, S., and Sawant, S. N. (2018). Functional alkoxysilane mediated controlled synthesis of Prussian blue nanoparticles, enabling silica alginate bead development; nanomaterial for selective electrochemical sensing. *Electrochimica Acta* 287, 37–48. doi:10.1016/j.electacta.2018.05.003

Pandey, P. C., Yadav, H. P., Shukla, S., and Narayan, R. J. (2021b). Electrochemical sensing and removal of cesium from water using prussian blue nanoparticle-modified screen-printed electrodes. *Chemosensors* 9, 253. doi:10.3390/chemosensors9090253

Park, B., Jung, J-E., Lee, H. U., Bae, J-S., Muruganantham, R., Huh, Y. S., et al. (2023). Generation of controllable patterned nano fibrous networks by electrospinning lithography: simultaneous detection and adsorption toward cesium ions. *ACS Sustain. Chem. Eng.* 11 (9), 3810–3819. doi:10.1021/acssuschemeng.2c06998

Park, B., Lee, M. Y., and Choi, S. J. (2023). Selective removal of cesium by magnetic biochar functionalized with Prussian blue in aqueous solution. *J. Radioanal. Nucl. Chem.* 332, 3335–3348. doi:10.1007/s10967-023-08986-2

Park, J. H., Kim, H., Kim, M., Lim, J. M., Ryu, J., and Kim, S. (2020). Sequential removal of radioactive Cs by electrochemical adsorption and desorption reaction using core-shell structured carbon nanofiber–Prussian blue composites. *Chem. Eng. J.* 399, 125817. doi:10.1016/j.cej.2020.125817

Qiu, M., Zhou, F., Sun, P., Chen, X., Zhao, C., and Mai, W. (2020). Unveiling the electrochromic mechanism of Prussian blue by electronic transition analysis. *Nano Energy* 78, 105148. doi:10.1016/j.nanoen.2020.105148

Rauwel, P., and Rauwel, E. (2019). Towards the extraction of radioactive cesium-137 from water via graphene/CNT and nanostructured prussian blue hybrid nanocomposites: a review. *Nanomaterials* 9, 682. doi:10.3390/nano9050682

Seema, H., Khan, N., Shah, A., Anwar ul, H., and Muhammad, A. (2023). Fabrication of self-assembled Prussian blue graphene hydrogel for highly selective removal of radioactive cesium in water: adsorption study. *Mater. Chem. Phys.* 306, 128003, 128003. doi:10.1016/j.matchemphys.2023.128003

Seema, H. (2020). Novel self-assembled magnetic Prussian blue graphene based aerogel for highly selective removal of radioactive cesium in water, *Arabian J. Chem.* 13, (2), 4417–4424. doi:10.1016/j.arabjc.2019.08.009

Vipin, A., Fugetsu, B., Sakata, I., Isogai, A., Endo, M., et al. (2016). Cellulose nanofiber backboned Prussian blue nanoparticles as powerful adsorbents for the selective elimination of radioactive cesium. *Sci. Rep.* 6, 37009. doi:10.1038/srep37009

Wang, P., Zheng, J., Ma, X., Xiao, D., Gao, F., Xiaogang, H., et al. (2020). Electroactive magnetic microparticles for the selective elimination of cesium ions in the wastewater. *Environ. Res.* 185, 109474, 109474. doi:10.1016/j.envres.2020.109474

Yasunari, T. J., Stohl, A., Hayano, R. S., Burkhart, J. F., Eckhardt, S., and Yasunari, T. (2011). Cesium-137 deposition and contamination of Japanese soils due to the Fukushima nuclear accident. *Proc. Natl. Acad. Sci. U. S. A.* 108, 19530–19534. doi:10.1073/pnas.1112058108

Yonekura, T., Okawada, M., and Yamataka, A. (2021). *Pediatric surgery*. Berlin, Heidelberg: Springer. doi:10.1007/978-3-662-43559-5_124

Zhou, W-Y., Sun, R., Li, S-S. G., Yuzheng, S., Wei, W., Jun, D., et al. (2021). Engineering surface electron and active site at electrochemical sensing interface of CN vacancy-mediated Prussian blue analogue for analysis of heavy metal ions. *Appl. Surf. Sci.* 564, 150131, 150131. doi:10.1016/j.apsusc.2021.150131